Adaptive solution of truss layout optimization problems with global stability constraints *

Alemseged Gebrehiwot Weldeyesus† Jacek Gondzio‡ Linwei He §
Matthew Gilbert¶ Paul Shepherd ‖ Andrew Tyas**

School of Mathematics and Maxwell Institute for Mathematical Sciences
The University of Edinburgh
Edinburgh EH9 3FD, United Kingdom

Technical Report ERGO-2019-001††

January 23, 2019

*Supported by EPSRC grant EP/N019652/1.
†A.Weldeyesus@ed.ac.uk
‡J.Gondzio@ed.ac.uk
§linwei.he@sheffield.ac.uk
¶m.gilbert@sheffield.ac.uk
‖P.Shepherd@bath.ac.uk
**a.tyas@sheffield.ac.uk
††For other papers in this series see http://www.maths.ed.ac.uk/ERGO/

Adaptive solution of truss layout optimization problems with global stability constraints

Abstract

Truss layout optimization problems with global stability constraints are nonlinear and nonconvex and hence very challenging to solve, particularly when problems become large. In this paper, a relaxation of the nonlinear problem is modeled as a (linear) semidefinite programming problem for which we describe an efficient primal-dual interior point method capable of solving problems of a scale that would be prohibitively expensive to solve using standard methods. The proposed method exploits the sparse structure and low-rank property of the stiffness matrices involved, greatly reducing the computational effort required to process the associated linear systems. Moreover, an adaptive 'member adding' technique is employed which involves solving a sequence of much smaller problems, with the process ultimately converging on the solution for the original problem. Finally, a warm-start strategy is used when successive problems display sufficient similarity, leading to fewer interior point iterations being required. We perform several numerical experiments to show the efficiency of the method and discuss the status of the solutions obtained.

Keywords
Truss structures Global stability Semidefinite programming Interior point methods

1 Introduction

Optimization of the layout of truss structures is a class of problem that has been studied for many decades, starting with the seminal paper of [30]. When solved computationally, truss layout optimization problems are usually formulated based on the ground structure approach ([11]), in which a set of nodes are distributed across the design space, then interlinked by potential connecting bars. The design variables in most cases are the cross-sectional areas of these bars, but may also include the coordinates of the nodes when geometry optimization is used ([40]).

The most common objectives of the optimization are to minimize the volume of the truss or to minimize its compliance, for which several formulations exist, ranging from linear programming, for example for the plastic design formulation, to nonlinear programming when elastic compatibility constraints are involved ([22, 3, 4, 8, 39, 33]).

Even though the solutions obtained using the aforementioned classical formulations can give useful insights into potential layouts of truss bars in a structure for use in the early stage of the design process, the designs generated may fail to satisfy many practical requirements, and therefore may require extensive modification in the later stages of the design process. Hence, in order to improve the practicality of the designs generated by layout optimization, researchers have sought to introduce many practical engineering issues in the formulation, such as constraints on stresses ([23, 19, 37, 38]), constraints on local buckling based on the Euler formula involving continuous ([46, 2, 34, 20, 18]) or discrete ([29]) variables, addressing global stability via the use of nominal forces ([43, 10]) or via introduction of global stability constraints ([6, 27, 36, 12, 42]), to mention a few. In recent years several articles have considered optimization of beam/frame structures with buckling constraints ([41, 28, 31]).

The aforementioned contributions which include Euler buckling constraints are intended to avoid slender bars in compression being included in the solution while including nominal forces are designed to ensure nodes connecting bars in compression are adequately braced. Formulations which directly include global stability constraints are concerned with ensuring the stability of the whole structure. This is of interest because, even if a structure is well-braced, it may fail as a result of insufficient overall elastic stiffness. Note that global stability problem formulations implicitly address the nodal instability problem, though do not take into account local instabilities of the sort dealt with by the Euler formula (e.g. [27]).

The focus of this paper is on problems with global stability constraints. These problems are in general formulated as nonlinear and nonconvex semidefinite programs ([6, 27, 36, 12]). Such problems are computationally challenging and for large-scale structures are usually considered numerically intractable, though software capable of solving small problems is available ([13, 25]). For this reason, some studies formulate the nonlinear semidefinite programming problem as an equivalent nonlinear programming problem ([42]). Nevertheless, in all approaches the size of problems that have been solved thus far in the literature have either been small or otherwise limited, e.g. by only specifying minimum connectivity between the nodes in the design space. This is in stark contrast to the plastic design formulation, solvable via linear programming, when full nodal connectivity problems can be solved even for high nodal densities.

In this article, we propose a relaxation of the nonlinear and nonconvex semidefinite programming formulation, for which we develop an efficient optimization algorithm based on interior point methods. The method is coupled with other novel techniques to make it capable of solving large-scale problems and with full nodal connectivity. The relaxed problem is still a semidefinite program but ignores the kinematic compatibility constraints present in standard elastic formulations. We observe huge computational gains by solving the relaxed formulation and provide lower bounds for the associated general nonlinear problems. Moreover, we report an estimation of the violation of the removed kinematics compatibility equations by solving an associated least-squares problem. For some small-scale benchmark problems, we additionally make comparisons between solutions of the relaxed and original nonlinear problems. In general, the error due to ignoring the kinematic compatibility equations are observed to be very small for reasonable values of the stability load factor, suggesting that solutions to the relaxed problems are acceptable. However, as we increase the value of the stability load factor beyond practically realistic values, we observe a high degree of violation in the compatibility equations and significant differences in the optimal designs. In this paper we also describe the techniques that contribute to the efficiency of the proposed solution algorithm.

Firstly, we employ the adaptive 'member adding' approach, previously used to solve plastic truss layout optimization problems ([15, 35, 44]) via linear programming, though now solving the problems of interest here via semidefinite programming. It is a procedure in which we approximate the large-scale original problem by a sequence of smaller subproblems, the solutions of which ultimately converge to that of the original problem. In the context of truss optimization, this is done by first solving the problem with minimum nodal connectivity, followed by generating and adding more members / bars based on degree of violation of constraints in the dual problem. The procedure continues until the solution to the original problems is obtained. This procedure greatly reduces the memory required to solve a given problem and, even using a standard desktop computer, we have managed to solve problems that otherwise would require hundreds of GB memory. Detailed statistics are presented in Section 6; see in particular the large-scale bridge example problem described in Section 6.3.1.

Secondly, similar to [7], we explicitly utilize the structures of the problems, i.e., the high degree of sparsity and low-rank property of the element stiffness matrices ([9, 5, 3, 8]), to address the computational bottle-neck associated with using the interior point method to solve semidefinite programming problems. This determines the coefficient matrix of the linear system originating in the algorithm. Roughly speaking, instead of performing $\mathcal{O}(mn^3 + m^2n^2)$ arithmetic operations ([14]), by using standard and straightforward expressions to determine the matrices involved in the linear systems, we perform $\mathcal{O}(m^2n)$ arithmetic operations, where m is the number of bars and n is number of nodal degrees of freedom. Note that, the sparsity of the element matrices is also effectively used in performing matrix inner products in the adaptive member adding procedure, as described in Remark 6.

Finally, as when solving the plastic truss layout optimization using the interior point method ([44]), we apply a warm-start strategy to solve some of the subsequent problems, determining an initial point that reduces the number of interior point iterations and overall improves the convergence of the optimization process. The technique relies on an observation that the number of newly added bars decreases towards the end of the adaptive member adding procedure and therefore the degree of similarity between successive subproblems increases at this stage.

The paper is organized as follows. In Section 2, we present the general nonlinear and nonconvex

semidefinite programming model of the truss layout optimization problem with global stability constraints, its relaxation, and the least-squares problem used to estimate violation of the elastic compatibility constraints. We describe the general framework of the primal-dual interior point method and exploitation of the structure of the matrices in Section 3 and the adaptive member adding procedure in Section 4. The warm-start strategy and related mathematical analysis are presented in Section 5 and the numerical experiments are described in Section 6. Finally, conclusions and possible future research directions are listed in Section 7.

2 The problem formulation with stability constraints

In this section, we describe the problem formulation for the layout optimization of trusses with global stability constraints. We use the 'ground structure' approach ([11]) to formulate problems. This is done by distributing a finite set of nodes, say d, across the design space and connecting these nodes by all possible potential bars, including overlapping ones. Hence, we have $m = d(d-1)/2$ bars, where clearly $m \gg d$. We denote the cross-sectional areas of the bars by a_i, $i = 1,...,m$. Let $f_\ell \in \mathbb{R}^n, \ell = 1,\ldots,n_L$ be a set of external forces applied to the structure where n ($\approx Nd$, N is the dimension of the design space, i.e., 2 or 3) is the number of the non-fixed degrees of freedom. Then, the associated (nodal) displacements $u_\ell \in \mathbb{R}^n$, $\ell = 1,\ldots,n_L$ satisfy the elastic stiffness equation

$$K(a)u_\ell = f_\ell,\ \ell = 1,\ldots,n_L, \tag{1}$$

where the stiffness matrix $K(a)$ is computed as

$$K(a) = \sum_{i=1}^{m} a_i K_i \tag{2}$$

and the element stiffness matrices K_i's are given by

$$K_i = \frac{E}{l_i}\gamma_i\gamma_i^T \tag{3}$$

with $\gamma_i \in \mathbb{R}^n$ being the vector of direction cosines for the ith bar.

Introducing the axial forces q_ℓ in member i which are given by

$$q_{\ell,i} = \frac{a_i E}{l_i}\gamma_i^T u_\ell \tag{4}$$

allows us to rewrite equation (1) as

$$Bq_\ell = f_\ell,\ \ell = 1,\ldots,n_L, \tag{5}$$

where $B = (\gamma_1,\cdots,\gamma_m) \in \mathbb{R}^{n\times m}$.

Next, we define the geometric stiffness matrix $G(q_\ell)$ as given by

$$G(q_\ell) = \sum_{i=1}^{m} q_{\ell,i}G_i, \tag{6}$$

where

$$G_i = \frac{1}{l_i}(\delta_i\delta_i^T + \eta_i\eta_i^T), \tag{7}$$

in which the vectors δ_i,η_i are determined so that γ_i, δ_i, η_i are mutually orthogonal; see [24] for details. The vectors δ_i and η_i are not necessarily unique. These are chosen in [24] as the orthogonal basis of the null space of γ_i^T and we follow similar approach in our implementation.

Now, the multiple-load case minimum weight truss layout optimization problem with global stability constraints can be formulated as

$$\begin{array}{ll} \underset{a,q_\ell,u_\ell}{\text{minimize}} & l^T a \\ \text{subject to} & \sum_i q_{\ell,i}\gamma_i = f_\ell, \qquad \forall \ell \\ & \frac{a_i E}{l_i}\gamma_i^T u_\ell = q_{\ell,i} \qquad \forall \ell \\ & -a\sigma^- \le q_\ell \le \sigma^+ a, \quad \forall \ell \\ & K(a) + \tau_\ell G(q_\ell) \succeq 0, \quad \forall \ell \\ & a \ge 0, \end{array} \tag{8}$$

where $l \in \mathbb{R}^m$ is a vector of lengths of the bars, and $\sigma^+ > 0$ and $\sigma^- > 0$ are the material yield stresses in compression and tension, respectively. Note that we can find a similar formulation to problem (8) in [42] with additional constraints enforcing local (Euler) buckling. The parameter τ_ℓ can be interpreted as a stability load factor and must be set to $\bar{\tau}_\ell \ge 1, \forall \ell$ to indicate that the resulting optimal structure is stable for the loads $\bar{\tau}_\ell f_\ell, \ell \in \{1, \ldots, n_L\}$.

It is worth mentioning that problem formulation (8) does not address local buckling, as addressed e.g., by the Euler buckling equation. Therefore, we can expect that the optimal design obtained by solving problem (8) could potentially include slender bars ([27]).

Due to the inclusion of the nonlinear kinematic compatibility equations (4), problem (8) is a nonlinear and nonconvex semidefinite programming problem. Such problems are in general very difficult to solve. In [13] and [36] methods for treating nonlinear semidefinite programming problems are described in which a variant of formulation (8) is solved. These formulations are very attractive, but the challenge of solving large-scale problems still remains. In [42], problem (8) is transformed from a semidefinite programming problem to a standard nonlinear programming problem.

In this paper, we relax problem (8) by ignoring the kinematic compatibility constraint (4), and solve a semidefinite programming problem of very large dimension because we allow full nodal connectivity. Namely, we consider

$$\begin{array}{ll} \underset{a,q_\ell}{\text{minimize}} & l^T a \\ \text{subject to} & \sum_i q_{\ell,i}\gamma_i = f_\ell, \qquad \forall \ell \\ & -a\sigma^- \le q_\ell \le \sigma^+ a, \quad \forall \ell \\ & K(a) + \tau_\ell G(q_\ell) \succeq 0, \quad \forall \ell \\ & a \ge 0, \end{array} \tag{9}$$

which is a (linear) semidefinite program and can be interpreted as the plastic design formulation with global stability constraints. In our numerical experiments described in Section 6, we additionally report the maximum violation of the elastic compatibility constraints for the optimal designs obtained by solving the relaxed problem (9). This violation is estimated by solving the least-squares problem

$$\underset{u_\ell}{\text{minimize}} \quad \max_\ell \frac{1}{||q_\ell^*||^2} \sum_i \left(\frac{a_i^* E}{l_i}\gamma_i^T u_\ell - q_{\ell,i}^*\right)^2, \tag{10}$$

where a^* and q_ℓ^* are the solution of the relaxed problem (9).

Note that the special case $\tau_\ell = 0, \forall \ell$, or in other words, excluding the matrix inequality constraints, reduces problem (9) to the plastic layout optimization problem, which is a linear program that can be solved efficiently by an interior point method ([44]).

Remark 1. The relaxed problem (9) belongs to the class of linear semidefinite programming problems. Hence, any of its solutions are also globally optimal solutions. Moreover, this provides a (strict) lower bound to nonconvex problem (8) for $\tau_\ell > 0$.

Remark 2. The relaxed problem (9) can be solved very efficiently by extending the adaptive 'member adding' scheme which has been used previously to solve large-scale plastic layout optimization of trusses formulated as linear programs ([15], [35], [44]).

Remark 3. For some of the examples in Section 6, we additionally solve the nonlinear semidefinite program (8) using a modified version of the method discussed in Section 3 and compare the solutions obtained with those of the linear SDP relaxation (9).

Remark 4. The least-squares problem (10) always has an objective value of zero for a single-load case problem and when $\tau = 0$ in (9). This is because for $\tau = 0$, the problem (9) precisely reduces to the so-called least-weight (or minimum volume) plastic design problem which has indeed been shown to be equivalent to the elastic minimum compliance problem ([22, 3, 4, 8, 1, 39]).

3 The primal-dual interior point framework

We adopt the Mehrotra-type primal-dual predictor-corrector interior point method ([14]) for semidefinite programming.

Introducing the slack variables s_ℓ^-, $s_\ell^+ \in \mathbb{R}^m_+$, and $S_\ell \in \mathbb{S}^n_+$, we rewrite (8) as

$$\begin{aligned}
\underset{a,q_\ell}{\text{minimize}} \quad & l^T a \\
\text{subject to} \quad & \sum_i q_{\ell,i}\gamma_i = f_\ell, && \forall \ell \\
& -a\sigma^+ + q_\ell + s_\ell^+ = 0, && \forall \ell \\
& -a\sigma^- - q_\ell + s_\ell^- = 0, && \forall \ell \\
& K(a) + \tau_\ell G(q_\ell) - S_\ell = 0, && \forall \ell \\
& S_\ell \succeq 0, s_\ell^+ \geq 0, s_\ell^- \geq 0, && \forall \ell \\
& a \geq 0,
\end{aligned} \tag{11}$$

and write down the following dual:

$$\begin{aligned}
\underset{\lambda_\ell, x_\ell^+, , x_\ell^-, x_a, X_\ell}{\text{maximize}} \quad & \sum_\ell f_\ell^T \lambda_\ell \\
\text{subject to} \quad & \sigma^+ \sum_\ell x_{\ell,i}^+ + \sigma^- \sum_\ell x_{\ell,i}^- + \sum_\ell K_i \bullet X_\ell + x_{a,i} = l_i, \forall i \\
& \gamma_i^T \lambda_\ell - x_{\ell,i}^+ + x_{\ell,i}^- + \tau_\ell G_i \bullet X_\ell = 0, && \forall \ell, \forall i \\
& X_\ell \succeq 0, && \forall \ell \\
& x_a \geq 0 \\
& x_\ell^+ \geq 0, x_\ell^- \geq 0, && \forall \ell,
\end{aligned} \tag{12}$$

where $\lambda_\ell \in \mathbb{R}^n$ denotes the virtual nodal displacement, x_ℓ^+, $x_\ell^+ \in \mathbb{R}^m, \ell = 1, \ldots, n_L$, $x_a \in \mathbb{R}^m$, $X_\ell \in \mathbb{S}^n_+$, and the notation $U \bullet V = \sum_i \sum_j U_{ij} V_{ij}$ for $U, V \in \mathbb{R}^{n \times n}$.

Remark 5. The primal problem formulation (11) is traditionally referred to as the dual problem, and the dual problem formulation (12) is traditionally referred to as the primal problem in literature on semidefinite programming ([45]).

Next, we introduce a barrier parameter $\mu > 0$ and formulate the perturbed first-order optimality conditions as

$$\sigma^+ \sum_\ell x^+_{\ell,i} + \sigma^- \sum_\ell x^-_{\ell,i} + \sum_\ell K_i \bullet X_\ell + x_{a,i} - l_i = 0, \qquad \forall i \tag{13a}$$

$$\gamma_i^T \lambda_\ell - x^+_{\ell,i} + x^-_{\ell,i} + \tau_\ell G_i \bullet X_\ell = 0, \qquad \forall \ell, \forall i \tag{13b}$$

$$\sum_i q_{\ell,i}\gamma_i - f_\ell = 0, \qquad \forall \ell \tag{13c}$$

$$-a\sigma^+ + q_\ell + s^+_\ell = 0, \qquad \forall \ell \tag{13d}$$

$$-a\sigma^- - q_\ell + s^-_\ell = 0, \qquad \forall \ell \tag{13e}$$

$$K(a) + \tau_\ell G(q_\ell) - S_\ell = 0, \qquad \forall \ell \tag{13f}$$

$$x^+_\ell \cdot s^-_\ell - \mu e = 0, \qquad \forall \ell \tag{13g}$$

$$x^-_\ell \cdot s^-_\ell - \mu e = 0, \qquad \forall \ell \tag{13h}$$

$$x_a \cdot a - \mu e = 0 \tag{13i}$$

$$X_\ell - \mu S^{-1}_\ell = 0, \qquad \forall \ell, \tag{13j}$$

where the notation $u \cdot v$, for any $v, u \in \mathbb{R}^m$ is a component wise multiplication and $e = (1, ..., 1)$ of appropriate size. We denote by $\xi_d = (\xi_{d_1}, \xi_{d_{2,\ell}})$ the negative of the dual infeasibilities (13a)-(13b), by $\xi_p = (\xi_{p_{1,\ell}}, \xi_{p_{2,\ell}}, \xi_{p_{3,\ell}}, \xi_{p_{4,\ell}})$ the negative of the primal infeasibilities (13c)-(13f), and by $\xi_c = (\xi_{c_{1,\ell}}, \xi_{c_{2,\ell}}, \xi_{c_3}, \xi_{c_{4,\ell}})$ the negative of the violation complementarity equations (13g)-(13j). Note that a direction obtained with the scaling corresponding to the last complementarity equation (13j) is called the HRVW/KSH/M direction ([21, 26, 32]).

Now, we solve system (13) for a sequence of $\mu_k \to 0$ to find the solution of the primal and dual problems (9) and (12). This is done by applying Newton's method to the optimality conditions (13) and solving the (reduced) linear system.

$$\begin{bmatrix} A_{11} & \tilde{A}^T_{12} & 0 \\ \tilde{A}_{12} & \tilde{A}_{22} & \tilde{B}^T \\ 0 & \tilde{B} & 0 \end{bmatrix} \begin{bmatrix} \Delta a \\ \Delta q_\ell \\ \Delta u_\ell \end{bmatrix} = \begin{bmatrix} \xi_1 \\ \xi_2 \\ \xi_3 \end{bmatrix}, \tag{14}$$

where (borrowing Matlab notation) $\tilde{B} = \text{blkdiag}(B, ..., B)$, $\tilde{A}_{22} = \text{blkdiag}(A_{11}, ..., A_{\ell\ell})$, and $\tilde{A}_{12} = (A_{11}, ..., A_{1\ell})^T$ with

$$\begin{aligned} (A_{11})_{ij} &= -\sum_\ell X_\ell K_i S^{-1}_\ell \bullet K_j + (D_{11})_{ij} \\ (A_{1\ell})_{ij} &= -X_\ell K_i S^{-1}_\ell \bullet G_j + (D_{1\ell})_{ij} \\ (A_{\ell\ell})_{ij} &= -X_\ell G_i S^{-1}_\ell \bullet G_j + (D_{\ell\ell})_{ij} \end{aligned} \tag{15}$$

and D_{kl} are diagonal matrices. The vector $(\xi_1, \xi_2, \xi_3)^T$ is the resulting right hand side. For complete description of the interior point method, we refer the reader to [14]. The rest of this section is dedicated to the computational difficulties associated with the interior point method for semidefinite programming and the techniques we use to resolve these difficulties.

There are several computational challenges associated with the linear system (14). Firstly, all block matrices $A_{kl}, k, l = 1, ..., n_L$ are dense and require a large amount of memory to store them; see Figure 1 for the sparsity structure of the coefficient matrix for a two load-case problem. Secondly, the straightforward computation of the coefficient matrix requires $\mathcal{O}(mn^3 + m^2n^2)$ operations ([14]).

The second challenge can be easily resolved by exploiting the low-rank property and sparsity of the data matrices $K_i, G_i, i = 1, ..., m$ ([7, 9, 5, 3, 8]). From (3) and (7), it can be seen that the rank of the element stiffness matrices $K_i, i = 1, ..., m$ is always 1 and the rank of the element geometric stiffness matrices $G_i, i = 1, ..., m$ is 1 for two-dimensional problems and 2 for three-dimensional problems. The direction

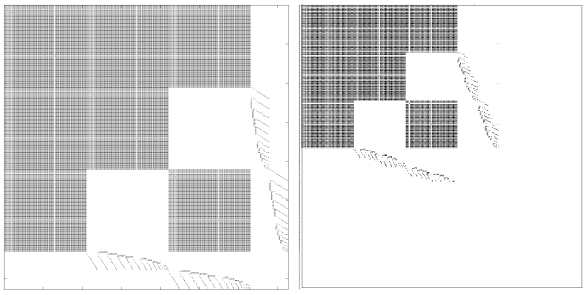

(a) (b)

Figure 1: Sparsity structure of the coefficient matrix in system (14) for a two load-case problem: (a) without adaptive member adding, number of non-zeroes = 73893; (b) with adaptive member adding, and in the final SDP iteration, number of non-zeroes = 24126.

cosines vectors γ_i, δ_i, and η_i are all very sparse with at most 4 or 6 nonzero entries for two- and three-dimensional problems, respectively. Therefore, we utilize this property to compute the coefficient matrix efficiently. For example, consider the block matrix A_{11} (single-load case for notation simplicity). We have

$$\begin{aligned}(A_{11})_{ij} - (D_{11})_{ij} &= -XK_iS^{-1} \bullet K_j \\ &= -\frac{E^2}{l_i l_j} X\gamma_i\gamma_i^T S^{-1} \bullet \gamma_j\gamma_j^T \\ &= -\frac{E^2}{l_i l_j} \gamma_j^T S^{-1}\gamma_i\gamma_i^T X\gamma_j,\end{aligned} \tag{16}$$

which can be computed in $\mathcal{O}(n)$ arithmetic operations and hence the computation of the coefficient matrix can be brought down to $\mathcal{O}(m^2 n)$.

In the next section, we discuss the novel approach employed to deal with the first challenge, i.e., the large memory requirements.

4 Adaptive 'member adding'

In problem formulation (9) we consider fully connected ground structures. Hence, for a $N-$dimensional problem comprising d nodes, the coefficient matrix of the reduced Newton system (14) has dimension

$$((n_L+1)m+n_Ln)\times((n_L+1)m+n_Ln),$$

where $m = d(d-1)/2$ and $n \approx Nd$. Moreover, all of the larger blocks of the coefficient matrix, each with dimension $m \times m$, are full matrices. This indicates that it would be computationally prohibitive to store or factorize the matrix; see also the large-scale bridge example problem described in Section 6.3.1.

In order to overcome this we extend the adaptive 'member adding' approach initially proposed for linear plastic truss layout optimization problems by [15] and later used in other studies, for example by [35] and [44]. It is a strategy whereby the original large problem is solved by successively solving a number of smaller sub-problems, as will now be described.

First we start with a structure constituting minimum connectivity, for example with the structure shown in Figure 2a for two-dimensional problems and Figure 2b for three-dimensional problems, and let m_0 be the number of bars in the the initial structure. We denote by $K_0 \subset \{1,\ldots,m\}$ the set of indices of the bars for which the primal problem (11) and its dual (12) are currently solved. Next, we compute the dual violations using only variables λ_ℓ and X_ℓ in (12) which are described below.

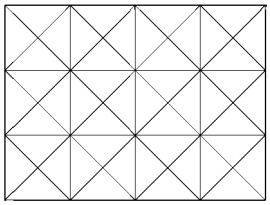

(a) two-dimensional problem

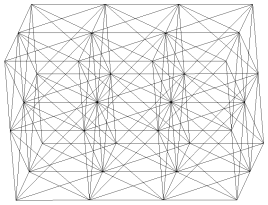

(b) three-dimensional problem

Figure 2: Initial minimally connected ground structures for: (a) two-dimensional problem, (b) three-dimensional problem.

For any member i to be dual feasible, see (12), we need

$$\sigma^+ \sum_\ell x^+_{\ell,i} + \sigma^- \sum_\ell x^-_{\ell,i} + \sum_\ell K_i \bullet X_\ell \leq l_i \tag{17a}$$

$$\gamma_i^T \lambda_\ell + \tau_\ell G_i \bullet X_\ell = x^+_{\ell,i} - x^-_{\ell,i}, \qquad \forall \ell \tag{17b}$$

$$X_\ell \succeq 0, \qquad \forall \ell \tag{17c}$$

$$x^+_\ell \geq 0, x^-_\ell \geq 0, \qquad \forall \ell. \tag{17d}$$

Now, since $x^+_\ell \geq 0$ and $x^-_\ell \geq 0$, from (17a) we have

$$\sum_\ell x^+_{\ell,i} \leq \frac{1}{\sigma^+}(l_i - \sum_\ell K_i \bullet X_\ell) \text{ and } \sum_\ell x^-_{\ell,i} \leq \frac{1}{\sigma^-}(l_i - \sum_\ell K_i \bullet X_\ell), \tag{18}$$

and from (17b) we have

$$-x^-_{\ell,i} \leq \gamma_i^T \lambda_\ell + \tau_\ell G_i \bullet X_\ell \leq x^+_{\ell,i}, \forall \ell. \tag{19}$$

Combining (18) and (19), we get

$$-\frac{1}{\sigma^-} \leq \frac{1}{l_i - \sum_\ell K_i \bullet X_\ell} \sum_\ell (\gamma_i^T \lambda_\ell + \tau_\ell G_i \bullet X_\ell) \leq \frac{1}{\sigma^+}, \forall \ell \tag{20}$$

for a member i to be dual feasible. Any member that violates (20) is said to be dual infeasible.

Now, solving the problem for members with indices in K_0, we use (20) to generate the set K as

$$K = \left\{ j \in \{1, \cdots, m\} \backslash K_0 | \frac{1}{l_j - \sum_\ell K_j \bullet X^*_\ell} \sum_{\ell=1}^{n_L} (\sigma^- \varepsilon^-_{\ell_j} + \sigma^+ \varepsilon^+_{\ell_j}) \geq 1 + \beta \right\}, \tag{21}$$

where

$$\varepsilon^+_{\ell_j} = \max\{(\gamma_j^T \lambda^*_\ell + \tau_\ell G_j \bullet X^*_\ell)), 0\}$$
$$\varepsilon^-_{\ell_j} = \max\{-(\gamma_j^T \lambda^*_\ell + \tau_\ell G_j \bullet X^*_\ell)), 0\}$$

with λ^*_ℓ and X^*_ℓ being optimal values, and $\beta > 0$ some prescribed tolerance. Then, we identify the bars with indices in K, filter them, and then finally add then to form the next problem. The purpose of the filtering is to limit the number of bars to be added in order to prevent fast growth of the size of the problem. For details of heuristic filtering approaches, see [44]. For the numerical experiments in Section 6 we use the member bar length approach described as filtering strategy AP3 in [44]. The member adding procedure terminates when $K = \emptyset$.

Remark 6. In our implementation, the sparsity of the data matrices K_j and G_j is exploited to determine the set K in (21) while performing the operations $K_j \bullet X^*_\ell$ and $G_j \bullet X^*_\ell$. Hence, this step becomes inexpensive. The CPU times reported for the numerical experiments in Section 6 include this procedure.

Remark 7. In Figure 1, we present the sparsity and size of the coefficient matrix of the reduced Newton system (14) for a small problem. Figure 1a shows the situation when the problem is solved for all potential bars, and Figure 1b shows the situation when we apply the adaptive member adding strategy. The sparsity structures may look similar but the size is reduced. Moreover, this reduction in size becomes even more significant for larger problems; see the large-scale bridge example problem described in Section 6.3.1.

5 Warm-start strategy

After performing several member adding iterations the subsequent sub-problems start to become more and more similar. Therefore, we use a warm-start strategy and determine an initial point that can reduce the number of interior point iterations required to obtain a solution. This has been used for the basic truss layout optimization problem formulated as a linear program in [44] and is now applied to the semidefinite programming formulations presented in this paper. The discussion in this section and the mathematical analysis closely follow Section 6 of [44].

As described in Section 4, we generate the set K in (21) at every member adding iteration. If $K \neq \emptyset$, then we form the new problem in which the variables are

$$\begin{aligned}(a, q_\ell, S_\ell, s_\ell^+, s_\ell^-) &\to (a, \bar{a}, q_\ell, \bar{q}_\ell, S_\ell, s_\ell^+, \bar{s}_\ell^+, s_\ell^-, \bar{s}_\ell^-)\\ (u, X_\ell, x_\ell^+, x_\ell^-) &\to (u, X_\ell, x_\ell^+, \bar{x}_\ell^+, x_\ell^-, \bar{x}_\ell^-).\end{aligned} \tag{22}$$

where the vectors with the super-bar, all in $\mathbb{R}^k$, $k = |K|$, represent the new variables corresponding to the newly added bars. We assume that the old solution (the left-hand-side in (22)) was feasible in the previous instance of the adaptive member adding scheme.

5.1 Computing a warm-start point

We set the initial point for the variables without the super-bar in the right hand side of (22) to the solution of the previous problem instance obtained with a loose tolerance. Following [16], the interior point algorithm should not be initialized at a point too close to the boundary of the feasible region. For the newly added variables, i.e., those with bars in (22), we use a specialized initialization procedure given below. We first set $\bar{x}_\ell^+$ and $\bar{x}_\ell^-$ as

$$\begin{aligned}\bar{x}_{\ell,j}^+ &= \max\{\bar{\gamma}_j^T \lambda_\ell + \tau_\ell \bar{G}_i \bullet X_\ell, \mu_0^{\frac{1}{2}}\},\ \forall j \in K,\\ \bar{x}_{\ell,j}^- &= \max\{-\bar{\gamma}_j^T \lambda_\ell - \tau_\ell \bar{G}_i \bullet X_\ell, \mu_0^{\frac{1}{2}}\},\ \forall j \in K,\end{aligned} \tag{23}$$

where μ_0 is the value of the barrier parameter corresponding to the saved solution of the previous problem instance. Its value is computed as

$$\mu_0 = \frac{\sum_{\ell=1}^{n_L} (X_\ell \bullet S_\ell + {x_\ell^+}^T s_\ell^+ + {x_\ell^-}^T s_\ell^-) + x_a^T a}{n_L \cdot n + (n_L + 1) m_0}, \tag{24}$$

where $m_0 = |K_0|$. Then, we set the new dual slack variable as

$$(\bar{x}_a)_j = \max\{|\bar{l}_j - \sigma^+ \sum_\ell \bar{x}_{\ell,j}^+ - \sigma^- \sum_\ell \bar{x}_{\ell,j}^- - \bar{K}_i \bullet X_\ell|, \mu_0^{\frac{1}{2}}\}, \forall j \in K. \tag{25}$$

Finally, new primal variables are defined by

$$\begin{aligned}\bar{q}_\ell^+ &= 0,\ \forall \ell\\ \bar{a}_j &= \mu_0 (\bar{x}_a^{-1})_j,\ \forall j \in K\\ \bar{s}_\ell^+ &= \sigma^+ \bar{a},\ \forall \ell\\ \bar{s}_\ell^- &= \sigma^- \bar{a},\ \forall \ell.\end{aligned} \tag{26}$$

Now, similar to [44], we estimate the bounds on the primal and dual infeasibilities, and the violation in complementarity slackness conditions induced by the new variables.

5.1.1 Primal infeasibility

We start with the bounds for the first three primal infeasibilties $\xi_{p_\ell} = (\xi_{p_{1,\ell}}, \xi_{p_{2,\ell}}, \xi_{p_{3,\ell}})$, $\ell = 1, ..., n_L$ (13c) -(13e).

$$\begin{aligned} ||\xi_{p_{1,\ell}}||_\infty &= ||f_\ell - \sum_i q_{\ell,i}\gamma_i - \sum_i \bar{q}_{\ell,i}\bar{\gamma}_i||_\infty \\ &= ||f_\ell - \sum_i q_{\ell,i}\gamma_i||_\infty \\ &= ||\xi^0_{p_{1,\ell}}||_\infty, \\ ||\xi_{p_{2,\ell}}||_\infty &= ||\sigma^+\bar{a} - \bar{q}_\ell - \bar{s}^+_\ell||_\infty = 0, \\ ||\xi_{p_{3,\ell}}||_\infty &= ||\sigma^-\bar{a} + \bar{q}_\ell - \bar{s}^-_\ell||_\infty = 0. \end{aligned} \tag{27}$$

Now, we determine the bound for the last primal infeasibility $\xi_{p_{4,\ell}}$ (13f).

$$\begin{aligned} ||\xi_{p_{4,\ell}}||_\infty &= ||-K(a) - \tau_\ell G(q_\ell) + S_\ell - \bar{K}(\bar{a}) - \tau_\ell \bar{G}(\bar{q}_\ell)||_\infty \\ &\leq ||\xi^0_{p_{4,\ell}}||_\infty + ||\bar{K}(\bar{a})||_\infty \\ &\leq ||\xi^0_{p_{4,\ell}}||_\infty + \mu_0^{\frac{1}{2}} \sum \frac{E_i}{\bar{l}_i}. \end{aligned} \tag{28}$$

This is because

$$\begin{aligned} ||\bar{K}(\bar{a})||_\infty &= ||\sum \frac{E_i\bar{a}_i}{\bar{l}_i}\bar{\gamma}_i\bar{\gamma}_i^T||_\infty \leq \sum \frac{E_i\bar{a}_i}{\bar{l}_i}||\bar{\gamma}_i\bar{\gamma}_i^T||_\infty \\ &= 2N\sum \frac{E_i\bar{a}_i}{\bar{l}_i} = \mu_0 \sum \frac{E_i\bar{x}^{-1}_{a,i}}{\bar{l}_i} \leq \mu_0^{\frac{1}{2}} \sum \frac{E_i}{\bar{l}_i}, \end{aligned} \tag{29}$$

where the last inequality above holds since $\bar{x}_{a,i} \geq \mu_0^{\frac{1}{2}}$ by definition. Moreover, $||\bar{\gamma}_i\bar{\gamma}_i^T||_\infty \leq 2N$. This is because, for example, when $N = 2$ the non-zeros entries of the direction cosine γ_i are γ_i=$(-\frac{(l_x)_i}{l_i}, -\frac{(l_y)_i}{l_i}, \frac{(l_x)_i}{l_i}, \frac{(l_y)_i}{l_i})$ which implies $||\bar{\gamma}_i\bar{\gamma}_i^T||_\infty \leq 4$. Therefore, the expressions in (27) and (28) demonstrate that primal infeasibility is at worst proportional to $\mu_0^{\frac{1}{2}}$, and hence insignificant.

5.1.2 Dual infeasibility

Starting from the second dual infeasibility $\xi_{d_{2,\ell}}$ in (13b), using (23), we have

$$(\xi_{d_{2,\ell}})_i = \bar{\gamma}_i^T\lambda_\ell - \bar{x}^+_{\ell,i} + \bar{x}^-_{\ell,i} + \tau_\ell\bar{G}_i \bullet X_\ell \leq \mu_0^{\frac{1}{2}}$$

and hence

$$||\xi_{d_{2,\ell}}||_\infty \leq \mu_0^{\frac{1}{2}}. \tag{30}$$

Now, we estimate the first dual infeasibilty ξ_{d_1} in (13a). Using the definition of $\bar{x}_a$ in (25) and the fact that $r - |r| \leq 2|r|, r \in \mathbb{R}$, we have

$$\begin{aligned} (\xi_{d_1})_i &= \bar{l}_i - \sigma^+\sum_\ell \bar{x}^+_{\ell,i} - \sigma^-\sum_\ell \bar{x}^-_{\ell,i} - \sum_\ell \bar{K}_i \bullet X_\ell - \bar{x}_{a,i} \\ &\leq 2|\bar{l}_i - \sigma^+\sum_\ell \bar{x}^+_{\ell,i} - \sigma^-\sum_\ell \bar{x}^-_{\ell,i} - \sum_\ell \bar{K}_i \bullet X_\ell| + \mu_0^{\frac{1}{2}} \\ &\leq 2(\bar{l}_i + \sigma^+\sum_\ell \bar{x}^+_{\ell,i} + \sigma^-\sum_\ell \bar{x}^-_{\ell,i} - \sum_\ell \bar{K}_i \bullet X_\ell) + \mu_0^{\frac{1}{2}} \\ &\leq 2(\bar{l}_i + \sigma_{max}\sum_\ell |\bar{\gamma}_j^T\lambda_\ell + \tau_\ell\bar{G}_i \bullet X_\ell| - \sum_\ell \bar{K}_i \bullet X_\ell) + (4n_L + 1)\mu_0^{\frac{1}{2}} \\ &= 2(\bar{l}_i + \sigma_{max}\sum_\ell (\varepsilon^-_{\ell_j} + \varepsilon^+_{\ell_j}) - \sum_\ell \bar{K}_i \bullet X_\ell) + (4n_L + 1)\mu_0^{\frac{1}{2}}, \end{aligned} \tag{31}$$

where $\sigma_{max} = \max\{\sigma^-, \sigma^+\}$, and ε_ℓ^- and ε^+ are given as (21). Hence,

$$||\xi_{d_1}||_\infty \leq ||2(\bar{l} + \sum_\ell \sigma_{max}(\varepsilon_\ell^- + \varepsilon_\ell^+) - \sum_\ell \bar{\mathscr{K}} X_\ell) + (4n_L + 1)\mu_0^{\frac{1}{2}} e||_\infty, \tag{32}$$

where $(\bar{\mathscr{K}} X_\ell)_j = \bar{K}_j \bullet X_\ell, \forall j \in K$. This expression reveals that there can be a considerable violation of the first dual constraint in (12) and so we apply the warm starting routine presented by [16, 17] to address this.

5.1.3 Centrality

We compute complementarity products for all newly added variables to evaluate the centrality of the new point. Note that the last centrality in condition (13) is automatically satisfied. Moreover, the pairs $(\bar{a}, \bar{x}_a)$ are μ_0 centered from (26).
Since

$$(\bar{x}_a)_j = \max\{|\bar{l}_j - \sigma^+ \sum_\ell \bar{x}_{\ell,j}^+ - \sigma^- \sum_\ell \bar{x}_{\ell,j}^- - \bar{K}_i \bullet X_\ell|, \mu_0^{\frac{1}{2}}\} \geq \mu_0^{\frac{1}{2}},$$

we have

$$\begin{aligned}
(\bar{x}_\ell^+)_j (\bar{s}_\ell^+)_j &= \sigma^+ (\bar{x}_\ell^+)_j \bar{a}_j = \mu_0 \sigma^+ \frac{(\bar{x}_\ell^+)_j}{(\bar{x}_a)_j} \leq \mu_0^{\frac{1}{2}} \sigma^+ (\bar{x}_\ell^+)_j \\
&= \mu_0^{\frac{1}{2}} \sigma^+ \max\{\bar{\gamma}_j^T \lambda_\ell + \tau_\ell \bar{G}_i \bullet X_\ell, \mu_0^{\frac{1}{2}}\} \\
&\leq \mu_0 \sigma^+ + \mu_0^{\frac{1}{2}} \sigma^+ |\bar{\gamma}_j^T \lambda_\ell + \tau_\ell \bar{G}_i \bullet X_\ell| \\
&= \mu_0 \sigma^+ + \mu_0^{\frac{1}{2}} \sigma^+ (\varepsilon_{\ell_j}^- + \varepsilon_{\ell_j}^+).
\end{aligned} \tag{33}$$

Next, finding upper bound on $(\bar{x}_a)_j$

$$\begin{aligned}
(\bar{x}_a)_j &= \max\{|\bar{l}_j - \sigma^+ \sum_\ell \bar{x}_{\ell,j}^+ - \sigma^- \sum_\ell \bar{x}_{\ell,j}^- - \bar{K}_i \bullet X_\ell|, \mu_0^{\frac{1}{2}}\} \\
&\leq \max\{\sigma_{max}(\sum_\ell (\bar{x}_\ell^+)_j + \sum_\ell (\bar{x}_\ell^-)_j) + \bar{K}_i \bullet X_\ell, \mu_0^{\frac{1}{2}}\} \\
&\leq \max\{\sigma_{max} n_L \max_\ell |\bar{\gamma}_j^T \lambda_\ell + \tau_\ell \bar{G}_i \bullet X_\ell| + 2n_L \mu_0^{\frac{1}{2}} + \bar{K}_i \bullet X_\ell, \mu_0^{\frac{1}{2}}\} \\
&\leq \sigma_{max} n_L \max_\ell |\bar{\gamma}_j^T \lambda_\ell + \tau_\ell \bar{G}_i \bullet X_\ell| + \bar{K}_i \bullet X_\ell + 2n_L \mu_0^{\frac{1}{2}},
\end{aligned}$$

we get

$$\begin{aligned}
(\bar{x}_\ell^+)_j (\bar{s}_\ell^+)_j &= \sigma^+ (\bar{x}_\ell^+)_j \bar{a}_j = \mu_0 \sigma^+ \frac{(\bar{x}_\ell^+)_j}{(\bar{x}_a)_j} \\
&= \mu_0 \sigma^+ \frac{\max\{\bar{\gamma}_j^T \lambda_\ell + \tau_\ell \bar{G}_i \bullet X_\ell, \mu_0^{\frac{1}{2}}\}}{(\bar{x}_a)_j\}} \\
&\geq \frac{\sigma^+ \mu_0^{\frac{3}{2}}}{(\bar{x}_a)_j} \\
&\geq \frac{\sigma^+ \mu_0^{\frac{3}{2}}}{\sigma_{max} n_L \max_\ell |\bar{\gamma}_j^T \lambda_\ell + \tau_\ell \bar{G}_i \bullet X_\ell| + \bar{K}_i \bullet X_\ell + 2n_L \mu_0^{\frac{1}{2}}} \\
&= \frac{\mu_0 \sigma^+}{\sigma_{max} n_L \mu_0^{\frac{-1}{2}} (\max_\ell (\varepsilon_{\ell_j}^- + \varepsilon_{\ell_j}^+) + \bar{K}_i \bullet X_\ell) + 2n_L}.
\end{aligned} \tag{34}$$

Then, using (33) and (34)

$$\frac{\sigma^+}{\sigma_{max} n_L \mu_0^{\frac{-1}{2}} (\max_\ell(\varepsilon_{\ell_j}^- + \varepsilon_{\ell_j}^+) + \bar{K}_i \bullet X_\ell) + 2n_L} \mu_0 \leq (\bar{x}_\ell^+)_j (\bar{s}_\ell^+)_j \leq \mu_0 \sigma^+ + \mu_0^{\frac{1}{2}} \sigma^+ (\varepsilon_{\ell_j}^- + \varepsilon_{\ell_j}^+),\ \forall j, \forall \ell. \quad (35)$$

Similarly,

$$\frac{\sigma^-}{\sigma_{max} n_L \mu_0^{\frac{-1}{2}} (\max_\ell(\varepsilon_{\ell_j}^- + \varepsilon_{\ell_j}^+) + \bar{K}_i \bullet X_\ell) + 2n_L} \mu_0 \leq (\bar{x}_\ell^-)_j (\bar{s}_\ell^-)_j \leq \mu_0 \sigma^- + \mu_0^{\frac{1}{2}} \sigma^- (\varepsilon_{\ell_j}^- + \varepsilon_{\ell_j}^+),\ \forall j, \forall \ell. \quad (36)$$

The bounds in (35) and (36) imply that the pairs $(\bar{x}_\ell^-, \bar{s}_\ell^-)$ and $(\bar{x}_\ell^+, \bar{s}_\ell^+)$, $\ell \in \{1, ..., n_L\}$ have no prominent outliers from the μ_0-centrality. This is due to the shift-like terms involving $(\varepsilon_{\ell_j}^- + \varepsilon_{\ell_j}^+)$ in the right hand side being multiplied by $\mu_0^{\frac{1}{2}}$, thus reducing the induced violation of the μ_0-centrality.

6 Numerical results

The interior point method has been implemented in MATLAB (R2016a). All numerical experiments have been performed using a PC equipped with an Intel(R) Core(TM) i5-4590T CPU running at 2.00 GHz with 16 GB RAM. For the case of the cold-start runs the initial points a^0, s_ℓ^{+0}, s_ℓ^{-0}, x_ℓ^{+0},x_ℓ^{-0}, x_a^+ are set to unity, S_ℓ, X_ℓ to the identity matrix I, and q_ℓ^0, λ_ℓ^0 to zero. The interior point algorithm terminates when

$$\frac{||\xi_p^k||_\infty}{1 + ||l||_\infty} \leq \varepsilon_p,\ \frac{||\xi_d^k||_\infty}{1 + ||\tilde{f}||_\infty} \leq \varepsilon_d,\ \frac{|l^T a^k - \sum_\ell f^T \lambda_\ell^k|}{1 + |l^T a^k|} \leq \varepsilon_{opt}, \quad (37)$$

where $\tilde{f} = (f_1, ..., f_{n_L})^T$, matrix terms are vectorized, and the primal and dual residuals ξ_p and ξ_d are given by (13). Note that, for feasible primal and dual points, the duality gap can easily be written as

$$l^T a - \sum_\ell f_\ell^T \lambda_\ell = \sum_\ell (x_\ell^{+T} s_\ell^+ + x_\ell^{-T} s_\ell^- + X_\ell \bullet S_\ell) + a^T x_a$$

by performing some elementary algebraic operations.
The primal and dual relative feasibility tolerances are set to $\varepsilon_p = \varepsilon_d = 10^{-6}$.

For the optimality tolerance, we use loose tolerances in the first few member adding iterations since the first few subproblems should not have to be solved to optimality, and then tighter tolerances in the final iterations, i.e., $\varepsilon_{opt} = [10^{-2}, 10^{-2}, 10^{-3}, 10^{-4}]$ and then always 10^{-5}. The reported CPU times correspond to the entire solution process, including the member adding computations.

In the original problems we consider all the potential bars, including overlapping bars. At the start of the solution process, we begin with the structure shown in Figure 2a for two-dimensional problems and Figure 2b for three-dimensional problems, and use $\beta = 0.001$ to generate the set of members in K given in (21) that are dual infeasible. If the warm-start strategy is used, then it is activated at the fourth member adding iteration or else before this if $(m_k - m_{k-1})/m_k \leq 0.12$, where m_k is the number of bars used in the kth member adding iteration. In applying this strategy, we use the solutions obtained with tolerance $\varepsilon_{opt} = 0.1$ in the preceding problem instance to determine the initial point of the subsequent problem.

For all examples, $\lambda_{\min}$ denotes the minimum eigenvalue of the generalized eigenvalue problem

$$(K(a) + \lambda_\ell G(q_\ell)) v_\ell = 0.$$

Moreover, we set $\tau_\ell = 0$ in (8) and (9) for problems without stability constraints and $\tau_\ell \geq 1$ for problems with stability constraints. Its specific values are mentioned in the examples below. Addtionally, when reporting the solution of the SDP relaxation (9), we also provide an estimate of the violation of the compatibility equations by solving the least-squares problem (10).

Table 1: L-shaped truss example: comparison of volumes obtained by solving the nonlinear SDP (8) and the SDP relaxation (9), and violation of the compatibility constraints (4) estimated by solving the least-squares problem (10).

τ	1	10	20	30	40	50	60	70	80	90
Nonlinear SDP volume (8)	0.0622	0.0646	0.0677	0.0717	0.0772	0.0846	0.0933	0.1031	0.1139	0.1251
Relaxed SDP volume (9)	0.0622	0.0643	0.0670	0.0703	0.0749	0.0805	0.0871	0.0947	0.1028	0.1117
Violation of compatibility (4), by (10)	5.0e-06	5.3e-04	0.0024	0.0066	0.0164	0.0306	0.0368	0.0459	0.0591	0.0702

Finally, we use Young's modulus $E = 210$GPa, and equal tensile and compressive strengths of 350MPa. In the plots of the optimal designs, bars in tension are shown in red and bars in compression are shown in blue (except for sake of clarity in the case of Figure 10). In all cases, the bars shown are those with cross-sectional area $\geq 0.001 a_{\max}$ and the dark dots are the active nodes connecting these bars.

6.1 Benchmark example problems

The objective of the examples in this section is to provide an insight into the solution obtained when a linear SDP relaxation (9) is solved for benchmark problems reported in the literature. This is done by comparing solutions with those obtained using nonlinear SDP (8), which includes compatibility constraints.

6.1.1 L-shaped truss example

We solve the benchmark L-shaped truss example problem shown in Figure 3a, comprising 132 bars. It has dimensions $1\text{m} \times 3\text{m} \times 4\text{m}$ (including the null region of dimensions $1\text{m} \times 2\text{m} \times 3\text{m}$), and each of the applied nodal loads is 350 KN, applied simultaneously. The optimal designs are given in Figures 3b-3f and resemble the solutions presented in [27, 42], who solved various problem formulations incorporating global stability constraints, and those presented in [43], [10], who obtained solved problems incorporating destabilizing nodal forces.

When the problem is solved without stability constraints, the solution shown in Figure 13b is obtained which comprises two parallel planar trusses. In that case the optimal design has volume 0.0620m^3 and $\lambda_{\min} = 1.2e-05 < 1$; hence it is not stable. Next, solving the relaxed problem (9) with stability constraints for $\tau_\ell = 1$, we obtain the solution shown in Figure 3c, where a connection between the two parallel planes is now established. The volume of the structure is 0.062217m^3 and $\lambda_{\min} = 1$. It is useful to now to establish an estimation of the violation of the elastic compatibility equation, obtained from (10); this is found to have a value of $4.9624e-06$. Moreover, we can compare the solution shown in Figure 3c to that of the optimal design shown in Figure 3d, obtained when solving the standard nonlinear SDP formulation (8). In this case the design has a marginally higher volume of 0.062241m^3.

In order to evaluate the result obtained by solving the relaxed SDP (9) and the nonlinear problem (8) in more detail, we also solve the problems for a larger value of the loading factor τ_ℓ. Thus for $\tau_\ell = 10$, the solution to the relaxed SDP gives the design shown in Figure 3e which has a volume 0.064333m^3 and the violation of the elastic compatibility equation is equal to $5.3177e-04$. This is larger than in the case above when $\tau_\ell = 1$. For $\tau_\ell = 10$ the nonlinear SDP gives the design shown in Figure 3f which has a somewhat larger volume, of 0.064639m^3. Table 1 shows the behaviour for even higher values of τ_ℓ, i.e., $\tau_\ell = 20, 30, ..., 90$. This indicates that when the value of τ is increased, the magnitude of the violation of the elastic compatibility constraints increases. Nevertheless, the results seem to agree for small values of τ_ℓ and especially for the required minimum value $\tau_\ell = 1$, so that the structure remains stable when the load is applied.

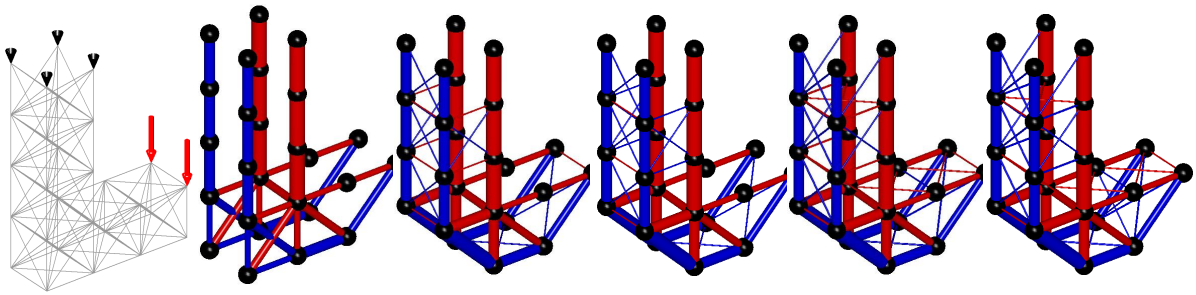

(a) (b) $\tau_\ell = 0$ in (9), vol = 0.062000m^3 (c) $\tau_\ell = 1$ in (9), vol = 0.062217m^3 (d) $\tau_\ell = 1$ in (8), vol = 0.062241m^3 (e) $\tau_\ell = 10$ in (9), vol = 0.064333m^3 (f) $\tau_\ell = 10$ in (8), vol = 0.064639m^3

Figure 3: L-shaped truss example: (a) design domain, boundary condition, and load; (b) optimal design without stability constraints; (c)-(f) optimal designs with stability constraints.

Remark 8. The solution to the problem without stability constraints presented in Figure 3a constitutes not only two independent planar trusses but also unstable nodes connecting bars that are in compression. The unstable nodes are stabilized in Figures 3c-3f with bracing bars.

6.1.2 Tower example

We solve the tower example problem shown in Figure 4a, comprising 1,953 bars in the fully connected ground structure. This is motivated by the similar problems solved by [36] and [43]. In this example, the tower is for sake of simplicity assumed to have dimensions of 1m $\times$ 1m $\times$ 3m, is fixed at its base, and is subjected to a downwards vertical load of 350KN at the centre of its upper surface.

The optimal design is shown in Figure 4b for the problem without stability constraints, which turns out to comprise six vertical inline bars with no bracing elements. Its volume is 0.00300m^3 and $\lambda_{\min} = 2.3277e-04$; clearly this structure is not stable. Now, setting $\tau_\ell = 1$ and solving the relaxed problem with stability constraints (9), we obtain the solution shown in Figure 4c with no intermediate unstable nodes, with bracing bars connecting the loaded node. The stable design has a volume of 0.003010m^3. Estimating the violation of the elastic compatibility equation we solve problem (10) and get $3.6617e-06$. The nonlinear formulation (8) produces the solution shown in Figure 4d and has a volume of 0.003020m^3.

For a higher value of $\tau_\ell = 10$, the solution to the relaxed SDP (9) returns the design shown in Figure 4e, with a volume 0.003102m^3 and compatibility constraint violation of $5.0965e-05$, and the nonlinear SDP (8) returns the design presented in Figure 4f with volume 0.003200m^3. Note that the results are in broad agreement with the results obtained by [36] and [43], where the tower problem is respectively solved using a nonlinear semidefinite formulation with global stability constraints and with the introduction of destabilizing nodal forces. In Table 2, results are presented for higher values of $\tau_\ell = 20,30,40$, where the largest violation of the compatibility equation is observed when $\tau_\ell = 40$. This suggests that further investigation is required to evaluate the practical validity of the solution of the relaxed SDP formulation (9) when large values of the stability load factor τ_ℓ is used.

Remark 9. As mentioned in Section 2, models (8) and (9) do not address local buckling. This is shown in in Figures 4c and 4f where long bars in compression are used as bracing or as means of stabilizing otherwise unstable nodes.

The purpose of this example is simply to demonstrate that if the bars in the optimal design are all in tension, then the solution obtained with or without the the global stability constraints are identical. To show this we solve the problem in Example 6.1.2 but with the direction of the load reversed, as shown in Figure 5a. The optimal design is shown in Figure 5b for the problem without stability constraints and once again comprises six vertical inline bars, all in tension and with no bracing elements. Its volume is 0.00300m^3 and $\lambda_{\min} = 426.5575 > 1$. This shows that the design is already stable and setting $\tau_\ell = 1$ and

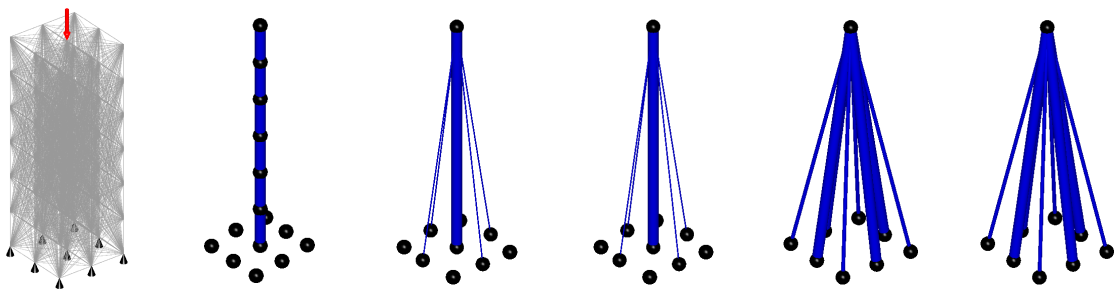

(a) (b) $\tau_\ell = 0$ in (9) , vol = 0.003000m^3 (c) $\tau_\ell = 1$ in (9), vol = 0.003010m^3 (d) $\tau_\ell = 1$ in (8), vol = 0.003020m^3 (e) $\tau_\ell = 10$ in (9), vol = 0.003102m^3 (f) $\tau_\ell = 10$ in (8), vol = 0.003200m^3

Figure 4: Tower example: (a) design domain, boundary conditions, and loading (downward); (b) optimal design without stability constraints; (c)-(f) optimal designs with stability constraints.

Table 2: Tower example: comparison of volumes obtained obtained by solving the nonlinear SDP (8) and the SDP relaxation (9), and violation of the compatibility constraints (4) estimated by solving the least-squares problem (10).

τ	1	10	20	30	40
Nonlinear SDP volume (8)	0.0030	0.0032	0.0370	0.0507	0.0663
Relaxed SDP volume (9)	0.0030	0.0031	0.0358	0.0499	0.0642
Violation of compatibility (4), by (10)	3.7e-06	5.1e-05	0.0151	0.0510	0.5889

re-solving the problem with stability constraints (9) will change neither its volume (which is is 0.00300m^3) nor its geometry, as can be seen in Figure 5c.

6.2 Adaptive 'member adding' problems

Here, we report on the efficacy of the adaptive member adding strategy described in Section 4 for the relaxed linear SDP (9). This is achieved by solving problems both with and without the strategy, verifying that the same solution is obtained, and reporting on comparative computational efficiency.

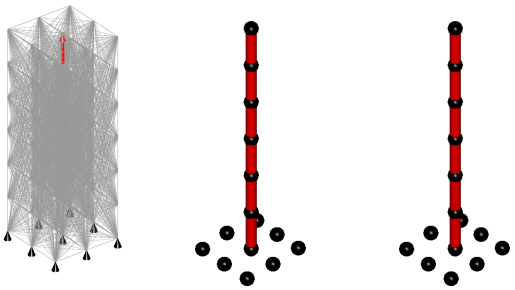

(a) (b) (c)

Figure 5: Tower example: (a) design domain, boundary conditions, and loading (now upward); (b) optimal design without stability constraints; (c) optimal design with stability constraints.

Table 3: Bridge example (small-scale): numerical statistics for the problem instance in Figure 6.

	Without member adding	With member adding
Volume (m^3)	0.05414	0.05414
Final no. of bars	3240	600
Mem. add. iter.	1	6
Total CPU (sec)	145	28

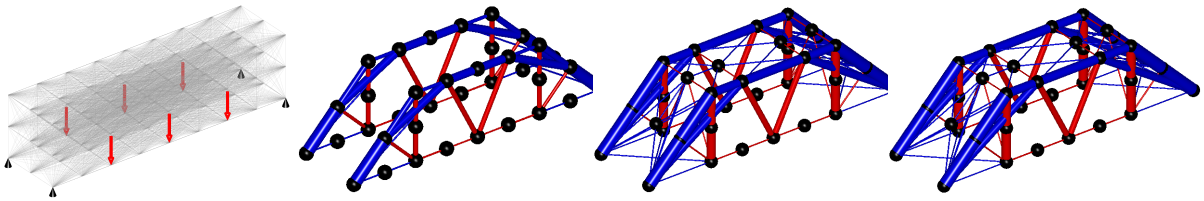

(a) (b) (c) (d)

Figure 6: Bridge example (small-scale): (a) design domain, boundary conditiond, and loading; (b) optimal design, without stability constraint; (c) optimal design, with stability constraint, without member adding; (d) optimal design, with stability constraint, with member adding.

6.2.1 Bridge example (small-scale)

We solve the bridge-like example problem shown in Figure 6a, comprising $3,240$ bars in the fully connected ground structure. The design domain has dimensions $8\text{m} \times 2\text{m} \times 2\text{m}$ and has fixed pin supports at each of the four corner nodes. Vertical loads of magnitude 350kN are applied to all nodes along each the two long edges at the base of the domain.

The solution obtained when stability constraints are not included is shown in Figure 6b, comprising two parallel planar trusses. In this case the optimal structure has a volume of 0.0540m^3 and $\lambda_{\min} = 3.8613e-08$ (i.e. clearly not stable). Next, we solve the problem with the stability constraint (9) for $\tau_\ell = 1$. Numerical results are shown in Table 3. Figure 6c shows the optimal design when solving the entire original problem and Figure 6d shows the structure obtained when member adding is used. The optimal designs are clearly identical, and have the same volume, equal to 0.05414m^3; see row 1 of Table 3. Moreover, the CPU times reported in the table illustrate the efficiency of the member adding scheme. In general, these efficiencies are much more pronounced for larger problems. Figure 7 illustrates the evolution of the solution when the adaptive member adding strategy is used, showing the potential bars and the corresponding optimal design for each member adding iteration. The violation of the elastic compatibility constraint is found to equal 5.8336e-06 at the end of the process.

6.3 Large-scale problems and warm-start strategy

We now solve a large-scale problem in which we additionally demonstrate the numerical benefit of using the warm-start strategy described in Section 5.

6.3.1 Bridge example (large-scale)

We consider again the bridge problem, though now with $90,100$ bars, as shown in Figure 9a; the loading conditions and dimensions are as described in Section 6.2.1. It is worth mentioning that if we attempted to solve the original problem without member adding, then we would need approx. 240GB of memory to store the coefficient matrix in (14). However, by applying the adaptive member adding technique we not only reduce the CPU time but also significantly reduce peak memory requirements. Numerical results

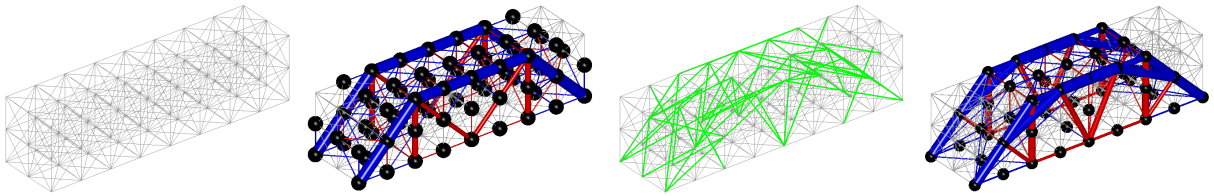

(a) Mem add iter.=1, 444 bars, vol= 0.05681m^3

(b) Mem add iter.=2, 518 bars, vol= 0.05429m^3

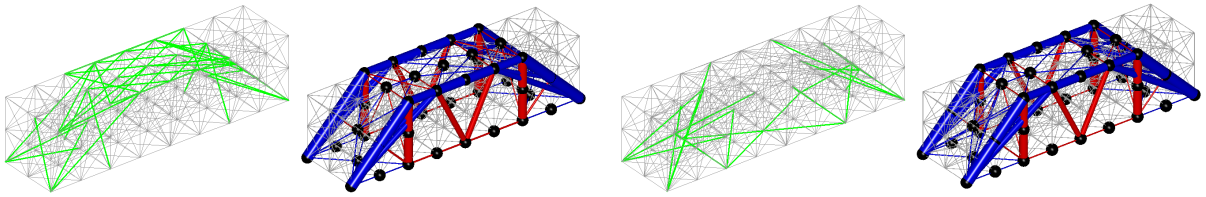

(c) Mem add iter.=3, 564 bars, vol= 0.05417m^3

(d) Mem add iter.=4, 588 bars, vol= 0.05414m^3

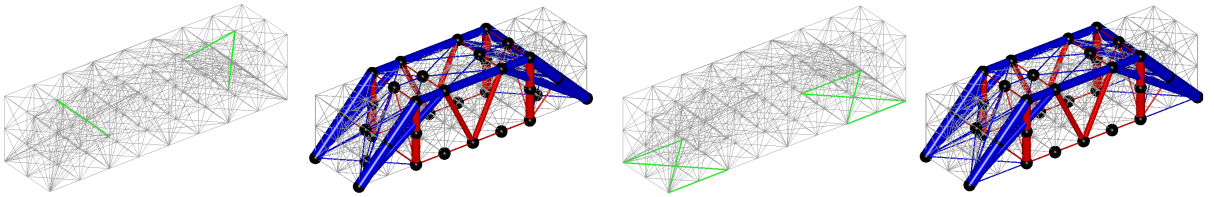

(e) Mem add iter.=5, 592 bars, vol= 0.05414m^3

(f) Mem add iter.=6, 600 bars, vol= 0.05414m^3

Figure 7: Bridge example (small-scale): potential bars and optimal designs illustrating the evolution of the optimal designs with respect to the member adding iterations reported in Table 3. Green bars represent newly added bars.

Table 4: Bridge example (large-scale): numerical statistics.

	Without warm-start	With warm-start
Volume (m^3)	0.05147	0.05147
Mem. add. iter.	7	7
Total CPU time (s), for entire optimization process	3638	2654

are presented in Table 4. It is evident that the warm-start strategy reduces CPU time by approx. 27%, which is achieved by cutting down the number of interior point iterations; see Figure 8. In this example, the warm-start is used in the last four member adding iterations. The optimal designs are shown in Figure 9, where Figure 9b shows the solution without stability constraints, which has a volume of 0.05122m^3 and $\lambda_{\min} = 8.0376e-08$ (i.e. clearly not stable). The last two Figures 9c and 9d correspond to stabilized designs obtained respectively without and with the warm-start strategy. The stable design has volume 0.05147m^3 in both cases, with violation of the elastic compatibility constraint equal to $5.2354e-06$.

6.4 Stadium-roof application with multiple load-cases

We solve the stadium roof design problem shown in Figure 10a. The roof is subject to three load-cases: LC1=f_1, LC2=f_1+f_2, and LC3=f_1+f_3, where the loads $f_1 = 0.27$kN/m^2, $f_2 = 2.7$kN/m^2, and $f_3 = 0.75$kN/m^2 are uniformly distributed. Note that the loads and dimensions have been simplified in the interests of clarity. The roof spans 40m in the y-direction, 80m in the x-direction and 4.2m in the the z-direction. Detailed dimensions are given in the caption of Figure 10a. The layout optimization problem has $36,856$ potential members.

We first solve the problem without stability constraints, obtaining the design shown in Figure 10b,

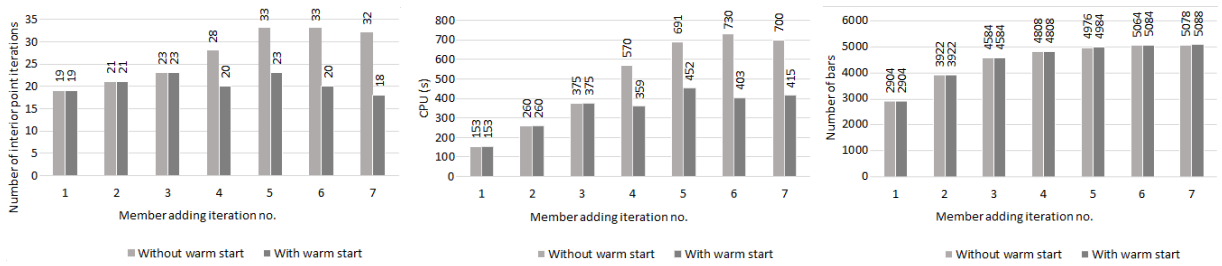

(a) (b) (c)

Figure 8: Bridge example (large-scale): comparison of (a) number of interior point iterations, (b) CPU times, and (c) problem sizes, when using cold-start and warm-start strategies. The warm-start was used in the last 4 member adding iterations.

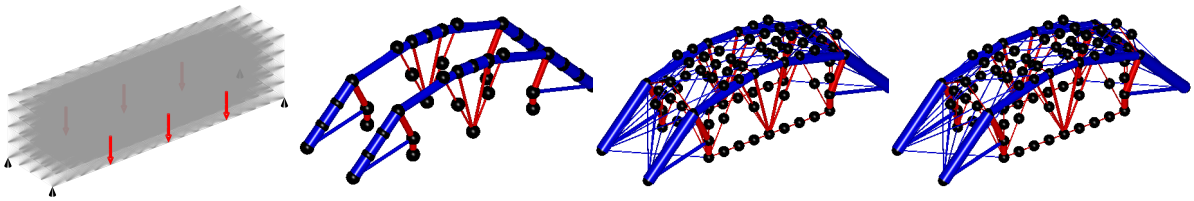

(a) (b) (c) (d)

Figure 9: Bridge example (large-scale): (a) design domain, boundary conditions, and loading; (b) optimal design without stability constraints; (c) optimal design with stability constraints and cold-start; (d) optimal design with stability constraints and warm-start.

comprising parallel disconnected planar trusses with a volume 2.2992m^3 and with minimum positive eigenvalues for the three load-cases LC1, LC2 and LC3 of $7.0387e-04$, $5.6185e-05$, and $1.8554e-04$, respectively. This indicates that the structure is not stable for all load-cases. Note that since this is a multiple load-case problem, we expect large violations of the elastic compatibility constraint, even for problems without the stability constraints, as mentioned in Remark 4. In this case, the violation was 0.0011. Next, we set $\tau_\ell = 10$, $\ell = 1,2,3$ and solve problem (9) with stability constraints to obtain the design shown in Figure 10c, where the parallel planar trusses are now connected. In this case, the volume of the structure is 2.3279m^3, only slightly higher than before. A total of 6 member adding iterations were required to obtain the solution and the final SDP problem solved contained 2487 members. The overall CPU time was 2238s. In this case the violation of the elastic compatibility equation (10) by the stable design was found to be 0.3190, which is large compared to the single-load case examples considered previously.

7 Conclusions

We have solved the truss layout optimization problem with global stability constraints via linear semidefinite programming by relaxing the nonlinear elastic compatibility constraint. A primal-dual interior point method has been used, tailored to solving these problems efficiently. The implementation utilizes the sparse structure and low-rank property of the element stiffness matrices to reduce the computational complexity to determine the linear systems arising in the algorithm. Moreover, we have extended the range of application of the adaptive member adding and warm-start techniques previously applied to truss layout optimization problems formulated as linear programs, so these can now be applied to problems modelled as semidefinite programs. By doing so, we have been able to find solutions to large-scale problems that could not have been solved using previously available methods and standard desktop computers.

We have demonstrated the validity of solutions of the relaxed problem by comparing them with solu-

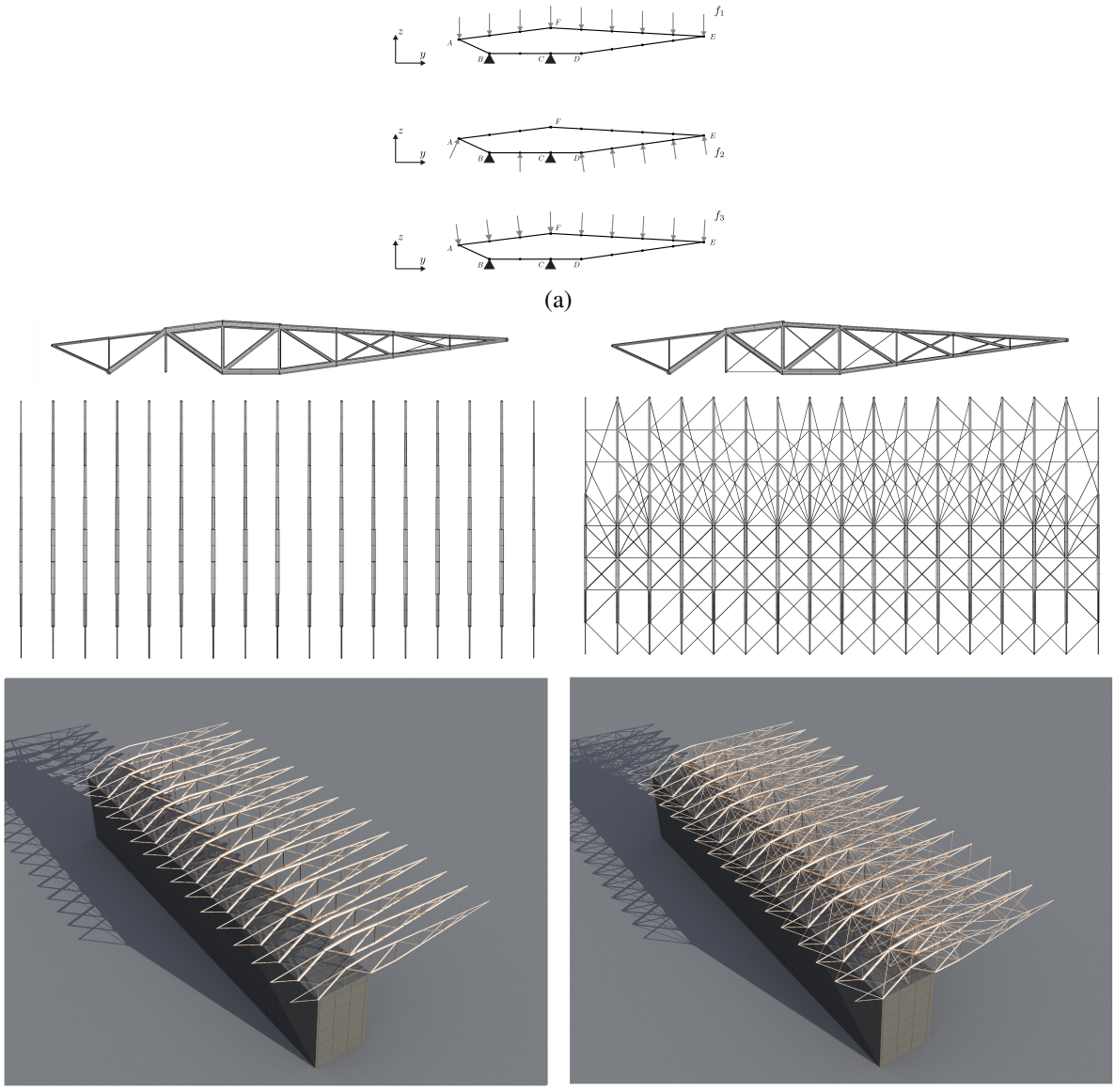

Figure 10: Stadium-roof application: (a) design domain, boundary conditions, and loads. $A = (0,0,2.3)$, $B = (0,5,0)$, $C = (0,15,0)$, $D = (0,20,0)$, $E = (0,40,2.8)$, $F = (0,15,4.2)$). The roof is 80m long in the x-direction; (b) optimal design without stability constraints; (c) optimal designs with stability constraints. Note that in the plots, the member sizes are scaled for good visual presentation.

tions of the original nonlinear problem for reasonable values of the stability load factor. If significantly higher stability load factors are to be used, beyond those usually employed in practice, then further investigation of the usefulness of the relaxed formulation should be undertaken.

Finally, direct methods were used to solve the linear systems arising from the interior point algorithm. The computational effort might be further reduced by use of iterative methods.

8 Acknowledgments

The research was supported by EPSRC, under grants EP/N019652/1, EP/N023471/1 and EP/N023269/1. The authors would also like to thank AECOM for providing information relating for the stadium case-study problem considered in Example 6.4.

9 Replication of results

The input and output data that are used for all of the examples described in Section 6 are explicitly provided there. The same material has been used in all examples and the material properties are reported right before Subsection 6.1. Note that these values and the applied loads require appropriate scaling if one wishes to use standard SDP solvers.

References

[1] W. Achtziger. Truss topology optimization including bar properties different for tension and compression. *Structural optimization*, 12(1):63–74, 1996.

[2] W. Achtziger. Local stability of trusses in the context of topology optimization part ii: A numerical approach. *Structural optimization*, 17(4):247–258, 1999.

[3] W. Achtziger, M. Bendsøe, A. Ben-Tal, and J. Zowe. Equivalent displacement based formulations for maximum strength truss topology design. *IMPACT of Computing in Science and Engineering*, 4(4):315–345, 1992.

[4] A. Ben-Tal and M. P. Bendsøe. A new method for optimal truss topology design. *SIAM Journal on Optimization*, 3(2):322–358, 1993.

[5] A. Ben-Tal and M. P. Bendsøe. A new method for optimal truss topology design. *SIAM Journal on Optimization*, 3(2):322–358, 1993.

[6] A. Ben-Tal, F. Jarre, M. Kočvara, A. Nemirovski, and J. Zowe. Optimal design of trusses under a nonconvex global buckling constraint. *Optimization and Engineering*, 1(2):189–213, 2000.

[7] A. Ben-Tal and A. Nemirovski. Robust truss topology design via semidefinite programming. *SIAM Journal on Optimization*, 7(4):991–1016, 1997.

[8] M. Bendsøe and O. Sigmund. *Topology Optimization: Theory, Methods and Applications*. Springer, 2003.

[9] M. P. Bendsøe, A. Ben-Tal, and J. Zowe. Optimization methods for truss geometry and topology design. *Structural optimization*, 7(3):141–159, 1994.

[10] R. F. C. Benot Descamps. The nominal force method for truss geometry and topology optimization incorporating stability considerations. *International Journal of Solids and Structures*, 51(13):2390 – 2399, 2014.

[11] W. Dorn, R. Gomory, and H. Greenberg. Automatic design of optimal structures. *Journal de Mécanique*, 3:25–52, 1964.

[12] A. Evgrafov. On globally stable singular truss topologies. *Structural and Multidisciplinary Optimization*, 29(3):170–177, 2005.

[13] J. Fiala, M. Kocvara, and M. Stingl. *PENLAB: a MATLAB solver for nonlinear semidefinite optimization*, 2013.

[14] K. Fujisawa, M. Fukuda, M. Kojima, and K. Nakata. *Numerical Evaluation of SDPA (Semidefinite Programming Algorithm)*, pages 267–301. Springer US, Boston, MA, 2000.

[15] M. Gilbert and A. Tyas. Layout optimization of large-scale pin-jointed frames. *Engineering Computations*, 20(8):1044–1064, 2003.

[16] J. Gondzio. Warm start of the primal-dual method applied in the cutting-plane scheme. *Mathematical Programming*, 83(1):125–143, 1998.

[17] J. Gondzio and P. González-Brevis. A new warmstarting strategy for the primal-dual column generation method. *Mathematical Programming*, 152(1):113–146, 2015.

[18] X. Guo, G. Cheng, and N. Olhoff. Optimum design of truss topology under buckling constraints. *Structural and Multidisciplinary Optimization*, 30(3):169–180, 2005.

[19] X. Guo, G. Cheng, and K. Yamazaki. A new approach for the solution of singular optima in truss topology optimization with stress and local buckling constraints. *Structural and Multidisciplinary Optimization*, 22:364–372, 2001.

[20] X. Guo, G. Cheng, and K. Yamazaki. A new approach for the solution of singular optima in truss topology optimization with stress and local buckling constraints. *Structural and Multidisciplinary Optimization*, 22(5):364–373, 2001.

[21] C. Helmberg, F. Rendl, R. J. Vanderbei, and H. Wolkowicz. An interior-point method for semidefinite programming. *SIAM Journal on Optimization*, 6(2):342–361, 1996.

[22] W. Hemp. *Optimum Structures*. Clarendon Press, 1973.

[23] U. Kirsch. On singular topologies in optimum structural design. *Structural Optimization*, 2:133–142, 1990.

[24] M. Kočvara. On the modelling and solving of the truss design problem with global stability constraints. *Structural and Multidisciplinary Optimization*, 23(3):189–203, Apr 2002.

[25] M. Kočvara and M. Stingl. PENNON: a code for convex nonlinear and semidefinite programming. *Optimization Methods and Software*, 18(3):317–333, 2003.

[26] M. Kojima, S. Shindoh, and S. Hara. Interior-point methods for the monotone semidefinite linear complementarity problem in symmetric matrices. *SIAM Journal on Optimization*, 7(1):86–125, 1997.

[27] R. Levy, H.-H. Su, and M. Kočvara. On the modeling and solving of the truss design problem with global stability constraints. *Structural and Multidisciplinary Optimization*, 26(5):367–368, Mar 2004.

[28] H. Madah and O. Amir. Truss optimization with buckling considerations using geometrically nonlinear beam modeling. *Comput. Struct.*, 192(C):233–247, 2017.

[29] K. Mela. Resolving issues with member buckling in truss topology optimization using a mixed variable approach. *Structural and Multidisciplinary Optimization*, 50(6):1037–1049, 2014.

[30] A. G. M. Michell. The limits of economy of material in frame structures. *Phil. Mag.*, 8(47):589–597, 1904.

[31] F. Mitjana, S. Cafieri, F. Bugarin, C. Gogu, and F. Castanié. Optimization of structures under buckling constraints using frame elements. *Engineering Optimization*, 2018.

[32] R. D. C. Monteiro. Primal-Dual Path-Following Algorithms for Semidefinite Programming. *SIAM Journal on Optimization*, 7(3):663–678, 1997.

[33] G. I. N. Rozvany, , T. Sokół, and V. Pomezanski. Fundamentals of exact multi-load topology optimization – stress-based least-volume trusses (generalized Michell structures) – Part I: Plastic design. *Structural and Multidisciplinary Optimization*, 50(6):1051–1078, 2014.

[34] G. I. N. Rozvany. Difficulties in truss topology optimization with stress, local buckling and system stability constraints. *Structural optimization*, 11(3):213–217, 1996.

[35] T. Sokół and G. I. N. Rozvany. On the adaptive ground structure approach for multi-load truss topology optimization. In *10th World Congresses of Structural and Multidisciplinary Optimization*, 2013.

[36] M. Stingl. *On the Solution of Nonlinear Semidefinite Programs by Augmented Lagrangian Method*. PhD thesis, Institute of Applied Mathematics II, Friedrich-Alexander University of Erlangen-Nuremberg, 2006.

[37] M. Stolpe and K. Svanberg. On the trajectories of the epsilon-relation relaxation approach for stress-constrained truss topology optimization. *Structural and Multidisciplinary Optimization*, 21:140–151, 2001.

[38] M. Stolpe and K. Svanberg. A note on tress-based truss topology optimization. *Structural and Multidisciplinary Optimization*, 25:62–64, 2003.

[39] M. Stolpe and K. Svanberg. A stress-constrained truss-topology and material-selection problem that can be solved by linear programming. *Structural and Multidisciplinary Optimization*, 27(1):126–129, 2004.

[40] K. Svanberg. Optimization of geometry in truss design. *Computer Methods in Applied Mechanics and Engineering*, 28(1):63 – 80, 1981.

[41] A. J. Torii, R. H. Lopez, and L. F. F. Miguel. Modeling of global and local stability in optimization of truss-like structures using frame elements. *Structural and Multidisciplinary Optimization*, 51(6):1187–1198, 2015.

[42] A. Tugilimana, R. Filomeno Coelho, and A. P. Thrall. Including global stability in truss layout optimization for the conceptual design of large-scale applications. *Structural and Multidisciplinary Optimization*, 57(3), 2018.

[43] A. Tyas, M. Gilbert, and T. Pritchard. Practical plastic layout optimization of trusses incorporating stability considerations. *Comput. Struct.*, 84(3-4):115–126, 2006.

[44] A. G. Weldeyesus and J. Gondzio. A specialized primal-dual interior point method for the plastic truss layout optimization. *Computational Optimization and Applications*, 2018.

[45] H. Wolkowicz, R. Saigal, and L. Vandenberghe. *Handbook of semidefinite programming. Theory, algorithms, and applications*. 2000.

[46] M. Zhou. Difficulties in truss topology optimization with stress and local buckling constraints. *Structural optimization*, 11(2):134–136, 1996.